remote sensing

MDPI

Article

Assessment of Vegetation Dynamics After South Sugar Loaf and Snowstorm Wildfires Using Remote Sensing Spectral Indices

Ibtihaj Ahmad * and Haroon Stephen

Civil and Environmental Engineering and Construction, University of Nevada Las Vegas, Las Vegas, NV 89154, USA; haroon.stephen@unlv.edu
* Correspondence: ahmadi1@unlv.nevada.edu

Abstract: Wildfires cause substantial ecological disturbances, altering vegetation dynamics and soil properties over extended periods. This study investigated the influence of vegetation burn severity on post-fire vegetation recovery rates using multi-temporal Landsat 8 surface reflectance imagery from 2014 to 2023. Two major fire events in Nevada, the Snowstorm Fire (2017) and the South Sugar Loaf Fire (2018), were examined through four spectral indices: the Normalized Difference Vegetation Index (NDVI), Moisture Stress Index (MSI), Modified Chlorophyll Absorption Ratio Index 2 (MCARI2), and Land Surface Temperature (LST). Statistical techniques, including the Mann–Kendall trend test and Linear Mixed Effects models, were applied to assess pre- and post-fire trends across burn severity classes. Results showed that vegetation recovery was primarily driven by temporal factors rather than burn severity, especially in the Snowstorm Fire. In the South Sugar Loaf Fire, significant changes were observed in LST and NDVI scores in low-severity areas, while MSI and MCARI2 scores exhibited significant recovery differences in high-severity zones. These findings suggest that post-fire vegetation dynamics vary spatially and temporally, with severity effects more pronounced in certain conditions. The study underscores the effectiveness of spectral indices in capturing post-disturbance recovery and supports their application in guiding site-specific restoration and long-term ecosystem management.

Keywords: vegetation recovery; post-fire assessment; wildfire impact analysis; post-fire vegetation monitoring

check for updates

Academic Editors: Guangsheng Chen, Zoltan Szantoi and Santonu Goswami

Received: 23 April 2025
Revised: 12 May 2025
Accepted: 15 May 2025
Published: 22 May 2025

Citation: Ahmad, I.; Stephen, H. Assessment of Vegetation Dynamics After South Sugar Loaf and Snowstorm Wildfires Using Remote Sensing Spectral Indices. *Remote Sens.* **2025**, *17*, 1809. https://doi.org/10.3390/rs17111809

Copyright: © 2025 by the authors. Licensee MDPI, Basel, Switzerland. This article is an open access article distributed under the terms and conditions of the Creative Commons Attribution (CC BY) license (https://creativecommons.org/licenses/by/4.0/).

1. Introduction

Wildfires are natural events that play a crucial role in forest ecosystems by facilitating nutrient replenishment in the soil and fostering new habitats for plants and animals. They can have negative impacts, which can significantly affect human health, air quality, and ecological processes, and play a role in climate change. In the western United States, wildfires have intensified and occurred more frequently in recent years due to anthropogenic climate change, leading to enduring effects such as changes in soil composition, air quality, vegetation patterns, and hydrological dynamics in affected regions.

Wildfires impact vegetation and soil; if severe, they can disturb the entire forest ecosystem, which can take years to recover, with effects varying temporally and spatially. Research indicates that wildfire impacts can endure in soil for up to eight decades, affecting vital ecological properties [1]. As reported for the Colorado Fort Range, recovery periods for infiltration capabilities can extend to seven years [2]. These impacts on soil affect vegetation regrowth and lead to excess runoff, with less infiltration causing flash floods and debris flows [3].

Post-fire vegetation recovery is critical to post-fire ecosystem recovery. Vegetation recovery is dependent on the temporal timeframe and severity of the fire. Temporal aspects of recovery can range from short-term responses within the first few years to long-term changes over decades [4]. Understanding these temporal changes is crucial for predicting ecosystem resilience and implementing effective post-fire management strategies.

The investigation of post-fire forest vegetation recovery is crucial due to forests' pivotal role in maintaining ecological stability, their capacity for carbon sequestration, and their importance as a defense against climate change hazards [5,6]. Understanding and supporting forest recovery after wildfires is a complex and critical endeavor with profound implications for ecological balance, carbon management, and climate resilience, making it essential for both research efforts and governmental agencies [7].

Remote sensing has emerged as a highly efficient tool for earth observations, monitoring vast landscapes by harnessing various frequencies of the electromagnetic spectrum. Leveraging multitemporal and multispectral imagery at diverse resolutions, it offers robust methodologies for monitoring disturbances in the ecosystem [6,8–10]. The remote sensing technologies for fire monitoring are utilized for three different temporal fire-effect phases: pre-fire conditions, active fire characteristics, and post-fire ecosystem responses. Post-fire disturbance and ecosystem recovery is carried out through a time series analysis of multitemporal imagery. Since the opening of the image archive when data became freely available in a highly calibrated format, Landsat became a popular method for change detection and observing the Earth's surface, ecosystem, and marine waters [11]. Landsat-based algorithms like Landtrendr, Continuous Change Detection Classification (CCDC), and Vegetation Change Tracker (VCT) are some of the commonly applied algorithms for post-fire vegetation change detection.

While numerous algorithms and approaches have been developed for the initial phases, there has to date been limited focus on evaluating appropriate remote sensing methods across the extensive spatial and temporal ranges of post-fire-affected environments and understanding the role of burn severity in post-fire-affected environments. This gap is particularly evident in characterizing and assessing the patterns of forest ecosystem responses to fire disturbances.

This study focuses on evaluating the temporal impacts of wildfires and vegetation burn severity on vegetation health using remote sensing spectral indices of the Normalized Difference Vegetation Index (NDVI), Moisture Stress Index (MSI), Modified Chlorophyll Absorption Ratio Index 2 (MCARI2), and Land Surface Temperature (LST), measuring the greenness, moisture, and chlorophyll of vegetation, respectively. This study tests the hypothesis that higher burn severity significantly delays vegetation recovery rates, while temporal factors (i.e., post-fire precipitation, microclimate stabilization, soil regeneration and nutrient cycling, temperature trends, etc.) play a dominant role in shaping long-term post-fire recovery trajectories. Several studies have been conducted on utilizing isolated spectral indices for damage assessment. This study combines vegetation health-related spectral indices, depicting key information related to fire damage to vegetation to comprehensively understand the temporal changes caused due to fire and burn severity classes.

2. Literature Review

Fire-induced ecosystem disturbance across a forest is observed through remote sensing by the changes occurring across the reflected electromagnetic spectrum of visible, near-infrared (NIR), shortwave-infrared (SWIR), and middle-infrared (MIR) wavelengths [10,12]. These spectral ranges exhibit strong responsiveness to soil and plant color (visible), chlorophyll, and moisture content (NIR and SWIR/MIR), which are the key elements altered by fire severity [7,9,13].

The Normalized Difference Vegetation Index (NDVI) is the most prominent and commonly utilized measure for quantifying the presence of green vegetation in the near-infrared wavelength range, as well as assessing chlorophyll absorption in the red wavelength range [14,15]. The NDVI is a measure of photosynthetic biomass and has been shown to correlate well with ecological parameters, such as the fraction of green vegetation cover [16] and Leaf Area Index [17]. The NDVI is sensitive to changes in vegetation conditions and has been shown to accurately detect forest disturbances. Even though we cannot consider the NDVI a direct measurement of productivity, it is tightly linked to photosynthetic active radiation (FPAR), which is a factor that regulates production [18–21]. Therefore, it can be used as an accurate proxy for vegetation dynamics after each fire.

The Modified Chlorophyll Adsorption Index 2 (MCARI2) spectral index is sensitive to chlorophyll concentrations in vegetation but insensitive to soil reflectance and possesses a strong correlation with the green Leaf Area Index (LAI) [22,23]. Leaf chlorophyll concentration is an indicator of plant nitrogen status, as nitrogen is critical to plant health and growth [24]. The LAI constitutes a significant ecological parameter with direct relevance to the process of vegetation recovery. This parameter offers insights into the biophysical mechanisms underlying vegetation and facilitates the anticipation of recovery dynamics [25]. Having a strong correlation with the LAI, nitrogen, and chlorophyll in plants and including a soil adjustment factor to reduce soil contamination effects, MCARI2 is an accurate proxy for understanding post-fire vegetation dynamics.

The Moisture Stress Index (MSI) is suitable for identifying water stress in plants that possess the ability to tolerate low leaf water content through cellular adjustments [9]. The MSI has also been proven to detect canopy stress and assess vegetation damage not detected by near-infrared (NIR)/red visible-based vegetation indices [26,27]. Canopy stress analysis is a crucial biophysical process in vegetation that helps researchers understand how vegetation responds to environmental changes [5]. The MSI can identify water stress in plants, and canopy stress can be utilized as a proxy for understanding post-fire vegetation moisture stress.

Land Surface Temperature (LST) refers to the temperature of the ground as it would feel when touched, also called the ground's "skin temperature" [28]. LST is among the foremost factors that govern the physical processes responsible for maintaining the balance of water, energy, and CO_2 on the land surface [29]. In the context of wildfire research, fire-induced changes to the land surface and the decrease in transpiration cause variations in the spatial distribution of LST [30].

3. Study Area and Data

The study focuses on two major wildfire events in northern Nevada: the Snowstorm Fire (2017) and the South Sugar Loaf Fire (2018). The Study Area Section 3.1 provides detailed descriptions of fire events and their ecological characteristics, while the Data Section 3.2 describes the datasets utilized, highlighting their relevance and utility in assessing post-fire vegetation.

3.1. Study Area

The Snowstorm Fire, ignited on 15 July 2017, burned 62,554 hectares (154,575 acres) and was controlled by 5 August 2017. The study area has an average annual temperature of 8 °C (46 °F) and an average annual precipitation of 698 mm. The aridity index is 0.43 for the area before the fire. The area is majorly dominated by the Colombia Plateau and Grassland, Inter-Mountain Basins Big Sagebrush Steppe, Inter-Mountain Basins Big Sagebrush Shrubland, and Great Basin and Intermountain Introduced Annual and Biennial

Forbland vegetation types. The area has a history of wildfires, notably the Winters Fire (2006), burning 96,577 hectares (238,648 acres).

Figure 1 provides imagery of pre- and post-fire conditions, and Table 1 describes the study points and the corresponding fire severity levels. The study points were selected on the criteria discussed in Methodology.

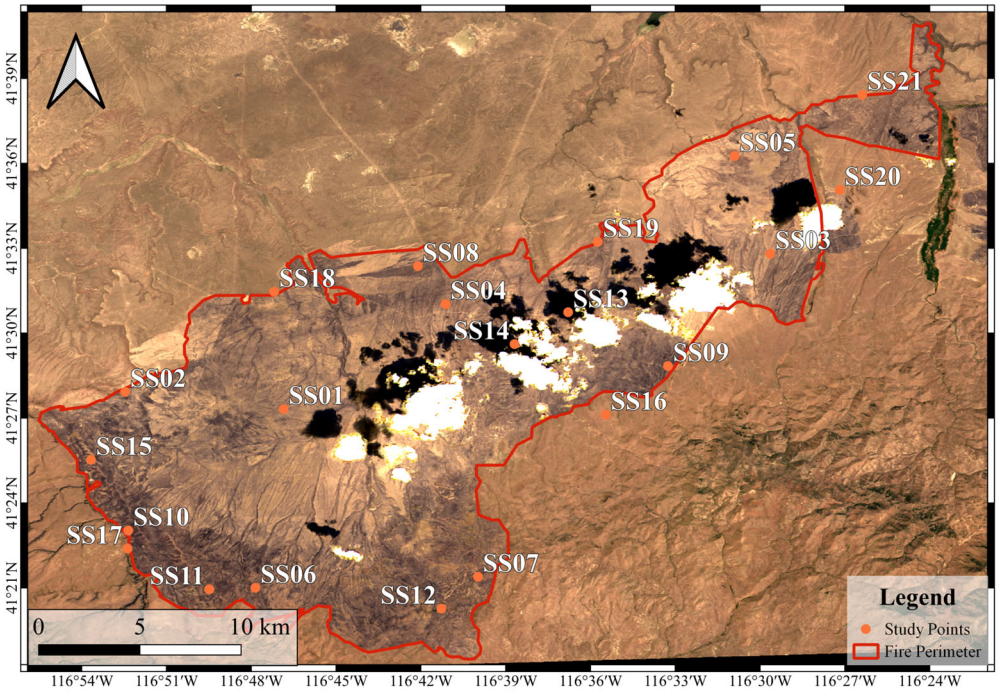

Figure 1. Figure represents a post-fire Landsat 8 OLI image obtained on 6 August 2017 for Snowstorm Fire area.

Table 1. Snowstorm fire study points and their burn severity levels.

Burn Severity Class	Study Points
Low severity (LS)	SS01, SS02, SS03, SS04, and SS05
Moderate–low severity (MLS)	SS06, SS07, SS08, SS09 and SS10
Moderate–high severity (MHS)	SS11, SS12, SS13, SS14, and SS15
Outside fire perimeter	SS16, SS17, SS18, SS19, SS20 and SS21

The South Sugar Loaf Fire, caused by lightning on 17 August 2018, burned 94,538 hectares (233,608 acres) before containment on 10 October 2018. It is characterized by shrubland and coniferous vegetation, with an annual precipitation of 344 mm, an average temperature of 8 °C (46 °F), and an aridity index of 0.2. Figure 2 provides imagery of pre- and post-fire conditions, and Table 2 describes the study points and the corresponding fire severity levels. The points were selected based on the criteria discussed in Methodology.

Table 2. South Sugar Loaf Fire study points and their burn severity levels.

Burn Severity Class	Study Points
Low severity (LS)	SSL01, SSL 02, SSL 03 and SSL 04
Moderate–low severity (MLS)	SSL 05, SSL 06, SSL 07 and SSL 08
Moderate–high severity (MHS)	SSL 09, SSL 10, SSL 11, and SSL 12
High severity (HS)	SSL13, SSL14, SSL15, and SSL16
Outside fire perimeter	SSL17, SSL18, SSL19, SSL20, and SSL21

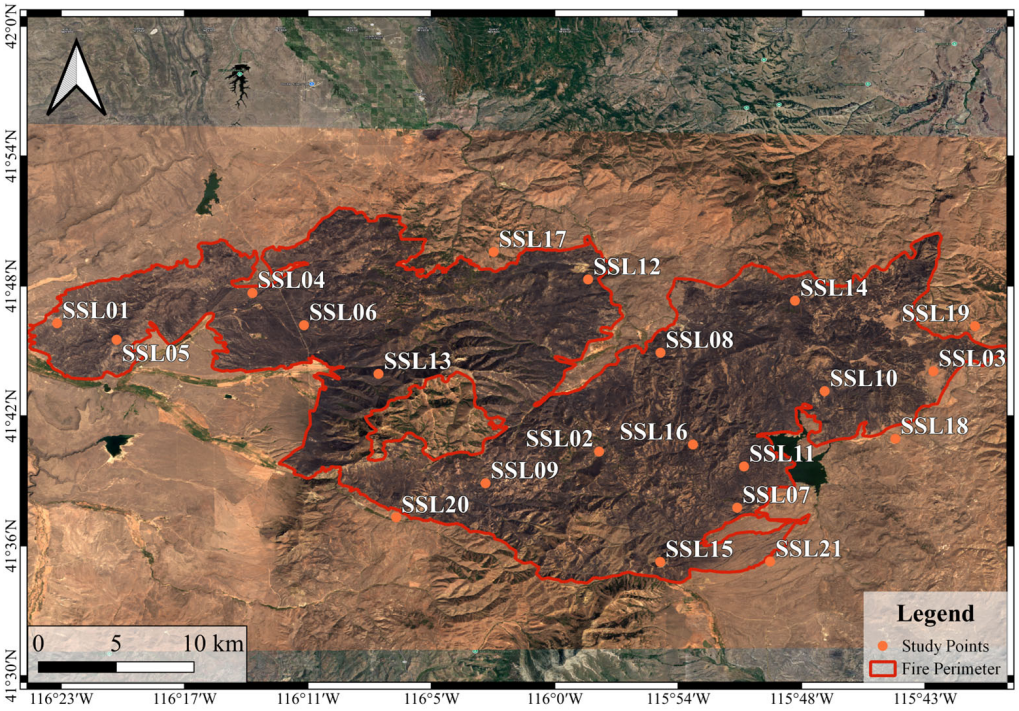

Figure 2. Figure represents a post-fire Landsat 8 OLI image obtained on 9 October 2018 for South Sugarloaf Fire area.

3.2. Data

Landsat 8 Tier 1 and Level 2 imagery was utilized to calculate spectral indices and assess vegetation dynamics. The images span the time period from January 2014 to December 2023. The Level 2 imagery is atmospherically, geometrically, and radiometrically corrected, providing surface reflectance information at a 30 m spatial resolution and a radiometric resolution of 12 bit. The 12-bit resolution enables each pixel to detect intensity from 0 to 4095, detecting very fine differences in the amount of reflected or emitted energy, making it suitable for detailed analyses of the Earth's surface. The image collection consists of 22 images per year, which were filtered for images in which study sites were being covered by cloud mass through Google Earth Engine, ensuring that only images without cloud cover and those belonging to the Landsat 8 OLI sensor were considered. A total of 198 images were present in the raw data.

4. Methodology

This study employed time-series analyses of Earth Observation (EO) datasets to assess the impacts of post-wildfire burn severity. Data processing and spectral index computations were carried out using the Google Earth Engine platform, while statistical analyses were performed in MATLAB R2023b. Landsat-8 OLI imagery was applied with cloud mask in Google Earth Engine to filter out all the cloudy images, and statistical indices were calculated on non-cloudy images. The spectral indices were then filtered for outliers, and only values within the spectral indices' ranges were kept, while others were removed, ensuring that only clean data were used for analysis. The methodology is summarized in Figure 3.

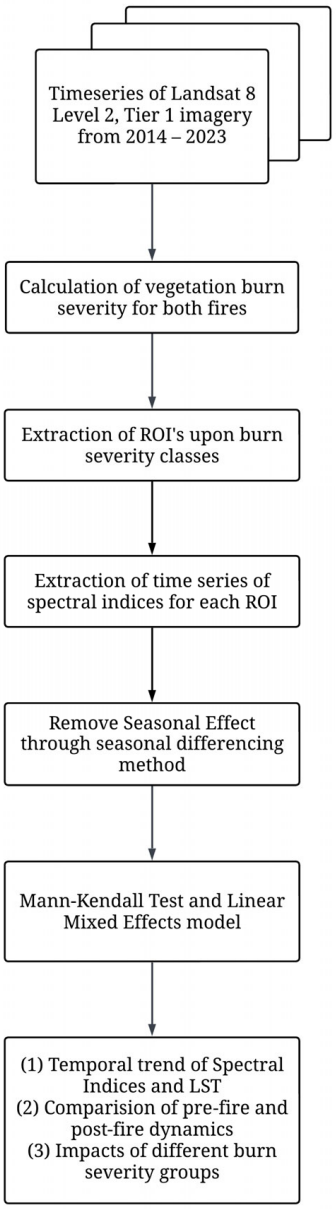

Figure 3. Flowchart illustrating the methodological framework, including data collection, preprocessing, and statistical analysis.

4.1. Spectral Indices

Vegetation burn severity was assessed using the Differenced Normalized Burn Ratio (dNBR), calculated using near-infrared (NIR) and shortwave infrared (SWIR) reflectance with immediate pre-fire and post-fire images. The dNBR was calculated for each fire on the dates mentioned of image acquisition for pre-fire and post-fire periods in the Study Area Section. The dNBR is calculated from the formula in Equation (1):

$$\mathrm{dNBR} = \mathrm{prefireNBR} - \mathrm{postfireNBR}. \quad (1)$$

The NBR is calculated from the formula in Equation (2) [31]:

$$\mathrm{NBR} = \frac{\mathrm{NIR} - \mathrm{SWIR}}{\mathrm{NIR} + \mathrm{SWIR}}, \quad (2)$$

where NIR is near-infrared, and SWIR is the shortwave infrared band of the OLI spectrum. Classification thresholds proposed by the [32] were applied to categorize burn severity, as illustrated in Table 3.

Table 3. Burn severity classification as proposed by USGS.

Severity Level	dNBR Values
Enhanced regrowth, high	(−0.5)–(−0.251)
Enhanced regrowth, low	(−0.25)–(−0.101)
Unburned	(−0.1)–0.099
Low severity	0.1–0.269
Moderate–Low severity	0.27–0.439
Moderate–High severity	0.44–0.659
High severity	0.67–1.30

The vegetation dynamics were quantified using the NDVI, MCARI2 and MSI, derived from red, green, near-infrared (NIR), and shortwave infrared 1 (SWIR1) bands, to monitor post-fire vegetation recovery through Equations (3)–(5) [9,33,34]:

$$\text{NDVI} = \frac{\rho_{\text{NIR}} - \rho_{\text{Red}}}{\rho_{\text{NIR}} + \rho_{\text{Red}}}, \text{and} \tag{3}$$

$$\text{MSI} = \frac{\rho_{\text{SWIR1}}}{\rho_{\text{NIR}}}, \text{and} \tag{4}$$

$$\text{MCARI2} = \frac{1.5\{2.5(\rho_{\text{NIR}} - \rho_{\text{Red}}) - 1.3(\rho_{\text{NIR}} - \rho_{\text{Green}})\}}{\sqrt{(2 * \rho_{\text{SWIR1}} + 1)^2 - \left(6 * \rho_{\text{SWIR1}} - 5\sqrt{\rho_{\text{Red}}}\right)} - 0.5}, \tag{5}$$

where ρ_{Red}, ρ_{Green}, ρ_{NIR}, ρ_{SWIR1} represent the red, green, near-infrared, and shortwave infrared 1 reflectance on the electromagnetic spectrum measured by the Landsat 8 satellite. LST was calculated in Kelvin using the Landsat 8 Level-2 Surface Temperature (ST) product, which is derived from Band 10 (thermal infrared) of the Landsat 8 Surface Reflectance product. This product, available in Google Earth Engine, provides pixel values that have already been atmospherically corrected and converted to land surface temperature (Kelvin) using the USGS operational preprocessing chain, including radiative transfer and surface emissivity corrections.

4.2. Study Site Selection

Study sites were stratified across burn severity levels using dNBR classifications, ensuring equal representation of severity levels and inclusion of unaffected areas. Randomly selected sites facilitated robust comparisons between burnt areas of different severity classes.

4.3. Removing Seasonal Effects

Seasonal variations, which are systematic fluctuations resulting from recurring environmental cycles such as precipitation and temperature changes, were removed from the NDVI, MCARI2, MSI, and LST datasets to isolate the underlying temporal trends. These seasonal patterns primarily represent short-term vegetation responses to environmental variability and provide useful insights within a single year. However, for the analysis of multi-year data, it is important to remove these seasonal components, as they can mask or interfere with the identification of longer-term ecological trends or recovery dynamics.

Time series decomposition was applied to differentiate seasonal patterns from long-term trends and irregular fluctuations, following established methodologies [35,36].

The seasonal fluctuations were removed through subtracting the weekly mean from the data approach. Weekly mean values were calculated for each week in the multi-year period; for instance, NDVI values of week 1 for every year in the time series were used to calculate the mean of week 1, which was subtracted from individual observations of week 1 throughout the time series. This approach was applied to every spectral index used in the study. The adjusted spectral indices' values were calculated using Equations (6) and (7), i.e.,

$$\text{Spectral Index}_{week} = \frac{1}{\text{n}}\sum_{i-1}^{\text{n}} \text{Spectral Index}_i, \text{ and} \quad (6)$$

$$\text{Spectral Index}_{residual_i} = \text{Spectral Index}_i - \text{Spectral Index}_{week}, \quad (7)$$

where Spectral Index$_i$ is the spectral index value for the ith observation within the same week and ID, and n is the number of spectral index observations within that week.

Outliers in the dataset were identified and removed using the Median Absolute Deviation (MAD) method, a robust statistical approach less sensitive to extreme values compared to mean-based measures. This technique calculates the median of the absolute deviations from the dataset's median and uses a threshold of 3.5 to flag potential outliers. MAD is particularly suitable for non-normally distributed data, ensuring the underlying data distribution remains representative after outlier exclusion [37].

4.4. Statistical Analysis

Statistical analysis employed non-parametric and mixed-effect modeling to examine temporal trends and the influence of burn severity on the NDVI, MSI, MCARI2 and LST. The Mann–Kendall test, a robust tool for detecting monotonic trends in non-normally distributed datasets, was applied to compare pre- and post-fire data [38,39]. The null hypothesis assumed no significant trends, and a p-value threshold of $p < 0.05$ was used to determine statistical significance. The rate of change was quantified using the Theil–Sen estimator [40], providing a non-parametric measure of trend magnitude.

Linear mixed-effect (LME) models analyze data by incorporating fixed effects (predictors) and random effects (group-level variability), making them suitable for hierarchical datasets. LME models account for dependencies and variability within grouped data, providing more robust conclusions [41,42]. This study selected LME models due to their ability to handle repeated measures and site-specific variability. Separate models were developed for every spectral index, with burn severity (categorical predictor: LHS, MHS, MLS, HS) and time (continuous predictor) as fixed effects. A random intercept for site ID accounted for site-specific variability. The restricted maximum likelihood (REML) was used for parameter estimation, and the model formula followed Equation (8),

$$\text{Y}_{ij} = \beta_0 + \beta_1 \text{X}_{burn\ severity} + \beta_2 \text{X}_{time} + \mu_i + \epsilon_{ij}, \quad (8)$$

where Y_{ij} represents the dependent variable (spectral indices) for the site i at time j, β_0 is the intercept, β_1 and β_2 are fixed-effect coefficients for burn severity and time, u_i is the random effect for site i, and ϵ_{ij} is the residual error.

Model fit was evaluated using the Akaike Information Criterion (AIC) and Bayesian Information Criterion (BIC), with lower values indicating better fit. Hypothesis testing employed ANOVA using Satterthwaite's method [43], and for predictors with statistically significant effects (p-value < 0.05), post hoc pairwise comparisons were conducted with Bonferroni corrections to assess differences between burn severity levels. Statistical analyses were performed in MATLAB.

5. Results

The analysis showed that dNBR values effectively captured post-wildfire burn severity across the study areas. The removal of seasonal components and a Mann–Kendall trend test revealed clear post-fire trends in the NDVI, MSI, MCARI2, and LST, with significant localized declines in vegetation indices and elevated land surface temperatures compared to pre-fire conditions. The relationship between burn severity and vegetation recovery indicated that higher severity areas experienced more pronounced and prolonged reductions in vegetation health.

5.1. Effects of Burn Severity

The dNBR analysis for the Snowstorm Fire revealed that 74.29% of the burned area (45,647 hectares) fell within the low-severity class. Moderate–low severity accounted for 10.92% (6705 hectares), moderately high severity comprised only 1.3% (796 hectares), and high severity comprised only 0.05% (29 hectares), while 38.27% (9325 hectares) of the fire-affected area was unburned from the fire. The dNBR map of the Snowstorm Fire is shown in Figure 4.

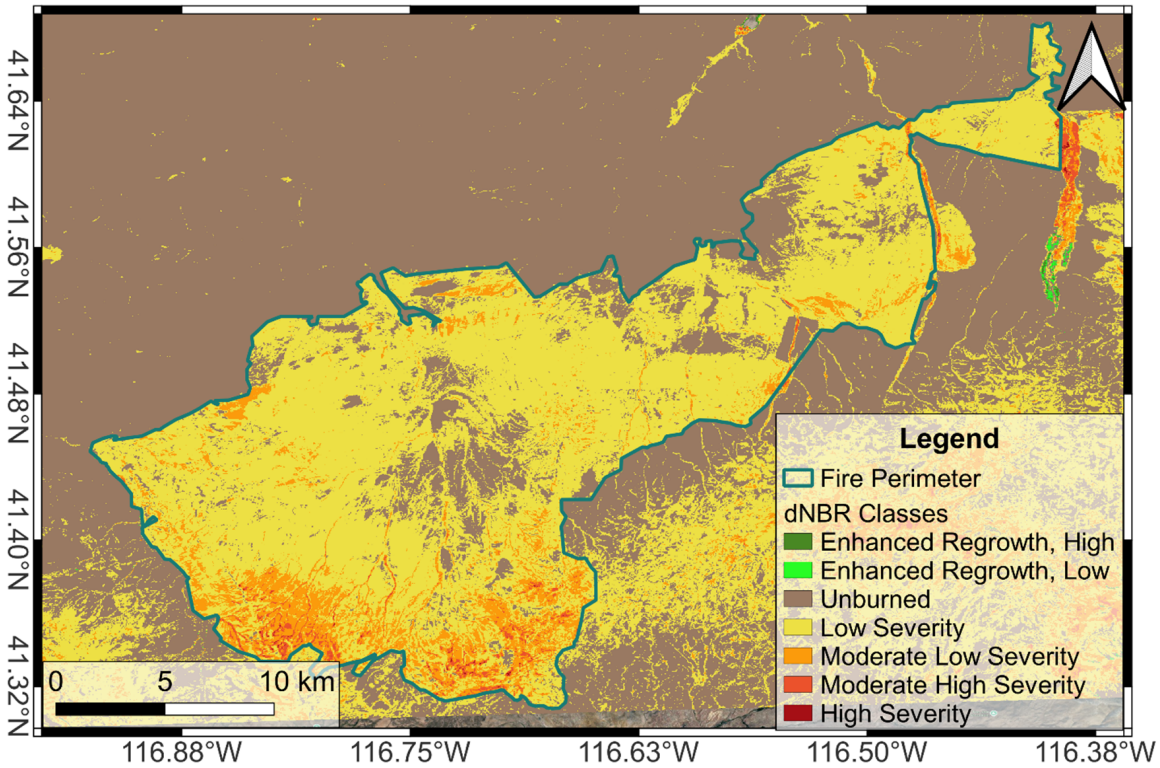

Figure 4. Classified dNBR map for the Snowstorm Fire.

In the South Sugar Loaf Fire, high-severity burns constituted 32% (39,288 hectares) of the affected area, while moderately high severity accounted for 33% (40,419 hectares). Moderate–low and low severity accounted for 22% (27,490 hectares) and 12% (14,345 hectares), respectively. The dNBR map of the South Sugarloaf Fire is shown in Figure 5.

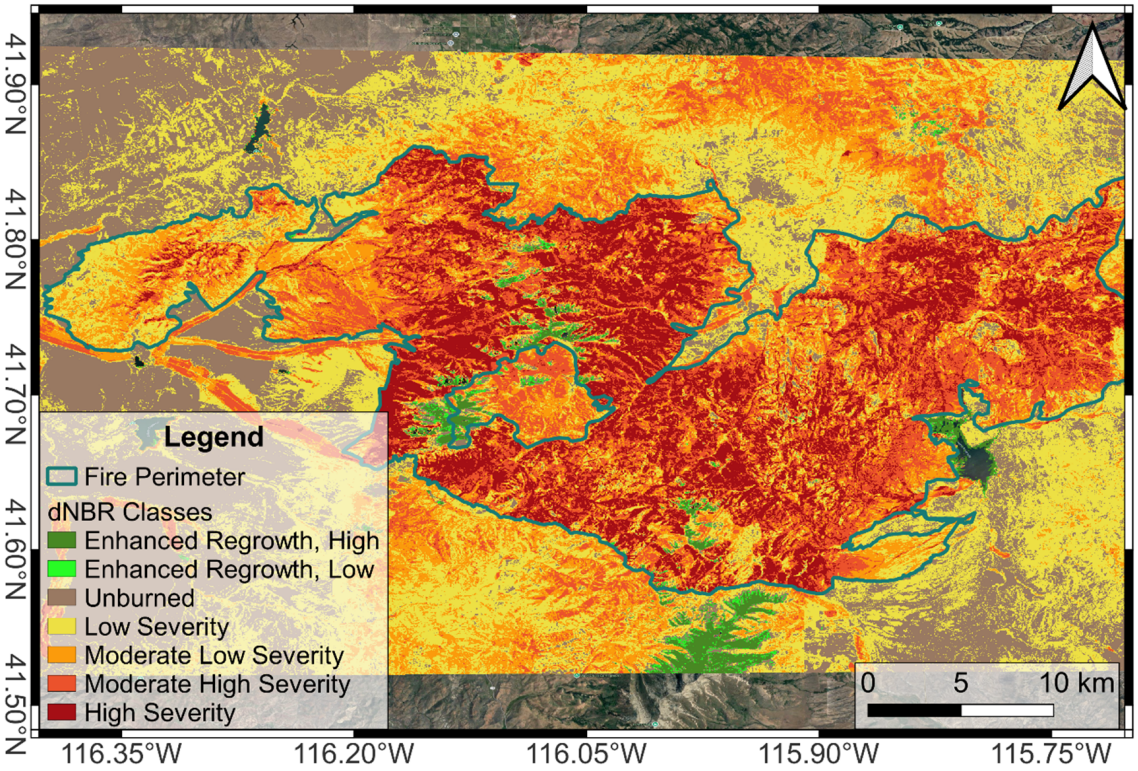

Figure 5. Classified dNBR map for the South Sugar Loaf Fire.

5.2. Trend Analysis of Spectral Indices

5.2.1. Snowstorm Fire

The Mann–Kendall test results for the Normalized Difference Vegetation Index (NDVI), Moisture Stress Index (MSI), Modified Chlorophyll Absorption Ratio Index 2 (MCARI2), and Land Surface Temperature (LST) were analyzed for multiple study sites, comparing trends in pre-fire and post-fire periods. Table 4 presents the statistical significance (*p*-value) and the magnitude of change (Sen's slope) for each index.

For the NDVI, pre-fire and post-fire trends were mostly insignificant, with *p*-values exceeding 0.05 across study sites. However, study sites 2, 8, 18, and 20 exhibited significant trends in the post-fire NDVI. The changes in Sen's slope post fire were visible across all study sites exhibiting a decrease in slope, indicating a decrease in vegetation cover following the fire.

MSI trends varied across study sites. Regarding the pre-fire MSI, 11 out of 21 study sites showed a significant trend. For the post-fire MSI, nine out of twenty-one study sites exhibited significant trends. Negative and decreasing Sen's slope values were common across multiple study sites, suggesting an overall reduction in moisture availability post disturbance.

MCARI2 trends were largely non-significant in both pre-fire and post-fire periods, as indicated by high *p*-values. However, isolated significant trends were observed, such as in study site 2 and 8 in post-fire MCARI2, suggesting potential localized vegetation stress changes.

LST exhibited non-significant trends across all study sites except for study sites 11 and 15 for pre-fire LST. While pre-fire values suggested stable conditions, post-fire LST values varied, with most sites showing increasing trends (positive Sen's slope). This variation reflects an increase in LST post fire and differences in local surface energy balance alterations due to fire effects.

Table 4. Mann–Kendall test results for Snowstorm Fire.

Study Site	Period	NDVI		MSI		MCARI2		LST	
		p-Value	Sen Slope	*p*-Value	Sen Slope	*p*-Value	Sen Slope	*p*-Value	Sen Slope
1	Pre-fire	0.0194	2.723×10^{-5}	0.0002	−0.00010	0.8088	1.3×10^{-6}	0.7348	−0.0009
	Post-fire	0.7409	1.217×10^{-6}	0.0123	−0.00004	0.2586	2.8×10^{-6}	0.3378	−0.0010
2	Pre-fire	0.2150	2.058×10^{-5}	0.0028	−0.00010	0.9309	-1.0×10^{-6}	0.6092	0.0012
	Post-fire	0.0100	1.575×10^{-5}	0.0005	−0.00007	0.0141	1.2×10^{-5}	0.2506	−0.0012
3	Pre-fire	0.0415	3.751×10^{-5}	0.5369	−0.00002	0.1269	1.6×10^{-5}	0.4214	−0.0015
	Post-fire	0.7484	2.160×10^{-6}	0.2600	−0.00002	0.4739	2.3×10^{-6}	0.8755	−0.0001
4	Pre-fire	0.0484	4.115×10^{-5}	0.0229	−0.00011	0.6317	7.2×10^{-6}	0.1065	−0.0036
	Post-fire	0.8082	1.450×10^{-6}	0.3187	−0.00002	0.5038	2.6×10^{-6}	0.5344	−0.0007
5	Pre-fire	0.2393	2.639×10^{-5}	0.8796	0.00001	0.7355	3.3×10^{-6}	0.2487	−0.0026
	Post-fire	0.9643	4.402×10^{-7}	0.7597	−0.00001	0.6545	2.0×10^{-6}	0.1653	0.0012
6	Pre-fire	0.0525	3.549×10^{-5}	0.0009	−0.00016	0.1586	1.8×10^{-5}	0.0709	−0.0036
	Post-fire	0.0948	1.140×10^{-5}	0.7224	−0.00001	0.8390	-7.8×10^{-7}	0.4410	0.0008
7	Pre-fire	0.0002	8.204×10^{-5}	0.0000	−0.00022	0.0095	3.7×10^{-5}	0.0577	−0.0038
	Post-fire	0.4816	4.855×10^{-6}	0.3413	−0.00003	0.8546	7.4×10^{-7}	0.5575	0.0005
8	Pre-fire	0.3605	1.620×10^{-5}	0.0000	−0.00014	0.5164	5.5×10^{-6}	0.4143	−0.0016
	Post-fire	0.0088	1.587×10^{-5}	0.0000	−0.00013	0.0192	8.6×10^{-6}	0.0534	−0.0020
9	Pre-fire	0.6909	9.990×10^{-6}	0.8506	−0.00001	0.7855	3.0×10^{-6}	0.1026	−0.0029
	Post-fire	0.3890	8.501×10^{-6}	0.0082	−0.00010	0.0566	9.5×10^{-6}	0.8260	−0.0002
10	Pre-fire	0.1139	3.122×10^{-5}	0.0038	−0.00015	0.1586	2.0×10^{-5}	0.4489	−0.0019
	Post-fire	0.8843	1.307×10^{-6}	0.2155	−0.00005	0.9723	1.4×10^{-7}	0.1776	−0.0014
11	Pre-fire	0.0598	5.111×10^{-5}	0.0000	−0.00027	0.0461	3.6×10^{-5}	0.0021	−0.0061
	Post-fire	0.7212	3.520×10^{-6}	0.9354	0.00000	0.0781	1.0×10^{-5}	0.3140	−0.0010
12	Pre-fire	0.0165	6.211×10^{-5}	0.0000	−0.00021	0.1196	3.2×10^{-5}	0.1466	−0.0037
	Post-fire	0.9987	4.095×10^{-8}	0.7232	−0.00001	0.4912	4.1×10^{-6}	0.9741	0.0000
13	Pre-fire	0.0273	2.595×10^{-5}	0.0627	−0.00007	0.1185	9.5×10^{-6}	0.1814	−0.0029
	Post-fire	0.2484	8.415×10^{-6}	0.0034	−0.00010	0.0221	9.0×10^{-6}	0.9856	0.0000
14	Pre-fire	0.2831	1.623×10^{-5}	0.2246	−0.00005	0.8980	1.0×10^{-6}	0.3220	−0.0018
	Post-fire	1.0000	1.085×10^{-8}	0.5551	−0.00001	0.5657	2.5×10^{-6}	0.7883	−0.0003
15	Pre-fire	0.0972	3.481×10^{-5}	0.0000	−0.00028	0.7125	5.0×10^{-6}	0.0112	−0.0051
	Post-fire	0.7922	2.303×10^{-6}	0.2364	−0.00005	0.6013	-2.0×10^{-6}	0.3432	−0.0009
16	Pre-fire	0.4025	2.171×10^{-5}	0.1944	−0.00007	0.2953	1.1×10^{-5}	0.2858	−0.0025
	Post-fire	0.2437	1.016×10^{-5}	0.1183	−0.00004	0.0140	1.0×10^{-5}	0.4907	0.0007
17	Pre-fire	0.0015	3.855×10^{-5}	0.0000	−0.00011	0.0113	1.4×10^{-5}	0.2858	−0.0018
	Post-fire	0.6071	3.339×10^{-6}	0.0483	0.00002	0.3925	-1.5×10^{-6}	0.1296	0.0011
18	Pre-fire	0.1323	2.593×10^{-5}	0.0000	−0.00019	0.4653	6.7×10^{-6}	0.7961	0.0006
	Post-fire	0.0042	1.730×10^{-5}	0.0000	−0.00020	0.0497	6.9×10^{-6}	0.1135	−0.0015
19	Pre-fire	0.1425	2.216×10^{-5}	0.4416	−0.00005	0.1400	1.2×10^{-5}	0.1914	−0.0031
	Post-fire	0.4642	5.246×10^{-6}	0.0000	−0.00008	0.0975	5.6×10^{-6}	0.9474	0.0001
20	Pre-fire	0.2555	2.921×10^{-5}	0.1833	−0.00008	0.3332	1.2×10^{-5}	0.3838	−0.0021
	Post-fire	0.0085	2.043×10^{-5}	0.0749	−0.00003	0.0026	1.2×10^{-5}	0.6237	0.0006
21	Pre-fire	0.1827	2.505×10^{-5}	0.4972	−0.00004	0.3268	1.2×10^{-5}	0.9199	−0.0002
	Post-fire	0.0588	1.723×10^{-5}	0.0303	−0.00005	0.0161	9.4×10^{-6}	0.3649	0.0008

Overall, the results highlight significant post-fire changes in the NDVI and MSI, with less pronounced trends in MCARI2 and LST. These findings suggest that fire has a notable impact on vegetation health and moisture availability, with implications for post-fire ecosystem recovery and resilience.

5.2.2. South Sugar Loaf

Mann–Kendall trend analysis was conducted for four spectral indices, the NDVI, MSI, MCARI2, and LST, on the South Sugar Loaf Fire study site to assess pre-fire and post-fire trends, with results summarized in Table 5, which presents the *p*-values and Sen's slope estimates for each index.

Pre-fire NDVI trends across sites had *p*-values mostly exceeding 0.1, indicating no significant trend. However, after the fire, NDVI *p*-values remained above 0.1 for most sites except for study sites 9, 13, and 19, with Sen's slope values generally increasing slightly post fire. This suggests that, while changes occurred in NDVI trends, they were not statistically significant at most sites, and post-fire vegetation recovery was in progress.

The Moisture Stress Index (MSI) exhibited consistent trends pre fire, with almost all locations, except for study sites 8, 10, 12, 14, and 19, exhibiting non-significant trends. Most post-fire study sites, 1, 5, 6, 7, 8, 9, 10, 11, 12, 14, 15, 16, and 19, exhibited significant trends, indicating that significant changes occurred, while most of the noted decreasing or negative Sen's slopes suggested that vegetation suffered with moisture stress.

MCARI2, which is sensitive to vegetation stress and canopy structure, showed statistically non-significant trends for most sites for pre-fire periods, except for 4, 5, and 19. In addition, the majority of sites in post-fire periods also exhibited non-significant trends, except for site 2, 9, 10, 12, 13, 16, and 19. The Sen's slope values, although small in magnitude, indicated a shift in vegetation structure in response to fire disturbance.

Land Surface Temperature (LST) trends showed no strong statistical significance before or after the fire, with *p*-values consistently above 0.1 for most sites, except for study sites 5 and 18 pre fire and study site 17 post fire. However, the Sen's slope values indicate minor shifts in LST, with both increasing and decreasing trends observed across different sites.

Overall, these results indicate that the South Sugar Loaf Fire induced observable, yet mostly statistically insignificant, changes in spectral indices. However, the variation in Sen's slope values suggests site-specific responses to fire disturbance.

Table 5. Mann–Kendall test results for South Sugar Loaf Fire.

Study Site	Period	NDVI		MSI		MCARI2		LST	
		p-Value	Sen Slope	*p*-Value	Sen Slope	*p*-Value	Sen Slope	*p*-Value	Sen Slope
1	Pre-fire	0.5264	6.3×10^{-6}	0.1309	4.7×10^{-5}	0.8966	6.7×10^{-7}	0.6376	−0.0007
	Post-fire	0.2826	1.2×10^{-5}	0.0001	-1.3×10^{-4}	0.3222	4.6×10^{-6}	0.4947	−0.0011
2	Pre-fire	0.1400	2.6×10^{-5}	0.0607	-4.1×10^{-5}	0.3573	3.9×10^{-6}	0.5821	0.0008
	Post-fire	0.3837	9.5×10^{-6}	0.4047	-1.9×10^{-5}	0.0113	8.4×10^{-6}	0.5877	0.0007
3	Pre-fire	0.2131	-1.6×10^{-5}	0.5010	-2.5×10^{-5}	0.5188	-4.0×10^{-6}	0.4884	−0.0008
	Post-fire	0.7871	2.2×10^{-6}	0.2732	2.4×10^{-5}	0.8731	-8.5×10^{-7}	0.5007	0.0007
4	Pre-fire	0.1056	-1.5×10^{-5}	0.3533	2.6×10^{-5}	0.0323	-1.0×10^{-5}	0.3861	−0.0012
	Post-fire	0.7000	-3.0×10^{-6}	0.0865	-4.4×10^{-5}	0.4531	2.3×10^{-6}	0.6925	0.0005
5	Pre-fire	0.3935	9.5×10^{-6}	0.9333	2.6×10^{-6}	0.0484	7.2×10^{-6}	0.0429	−0.0028
	Post-fire	0.9827	-1.7×10^{-7}	0.0000	-1.1×10^{-4}	0.6888	2.0×10^{-6}	0.8455	0.0002
6	Pre-fire	0.1147	-1.7×10^{-5}	0.0832	6.7×10^{-5}	0.1314	-7.7×10^{-6}	0.9794	0.0001
	Post-fire	0.6263	6.9×10^{-6}	0.0023	-1.5×10^{-4}	0.2192	7.0×10^{-6}	0.7067	−0.0003

Table 5. *Cont.*

Study Site	Period	NDVI		MSI		MCARI2		LST	
		p-Value	Sen Slope	*p*-Value	Sen Slope	*p*-Value	Sen Slope	*p*-Value	Sen Slope
7	Pre-fire	0.8258	$4.5 \times 10-6$	0.1690	-6.6×10^{-5}	0.2555	-6.4×10^{-6}	0.1374	−0.0029
	Post-fire	0.4441	1.1×10^{-5}	0.0150	-1.2×10^{-4}	0.1729	9.0×10^{-6}	0.7246	−0.0006
8	Pre-fire	0.6415	7.5×10^{-6}	0.0059	-1.0×10^{-4}	0.1772	7.9×10^{-6}	0.4727	−0.0012
	Post-fire	0.8666	1.5×10^{-6}	0.0005	-1.2×10^{-4}	0.3944	4.8×10^{-6}	0.9584	0.0001
9	Pre-fire	0.8190	4.1×10^{-6}	0.8436	-7.9×10^{-6}	1.0000	-1.9×10^{-7}	0.1443	−0.0027
	Post-fire	0.0023	3.9×10^{-5}	0.0213	-1.1×10^{-4}	0.0024	2.2×10^{-5}	0.5066	0.0012
10	Pre-fire	0.8939	-1.7×10^{-6}	0.0035	-1.4×10^{-4}	0.4186	5.0×10^{-6}	0.1854	−0.0026
	Post-fire	0.1552	2.4×10^{-5}	0.0000	-2.5×10^{-4}	0.0254	1.6×10^{-5}	0.4513	−0.0012
11	Pre-fire	0.6632	-8.2×10^{-6}	0.4186	-3.1×10^{-5}	0.3507	-6.9×10^{-6}	0.1576	−0.0030
	Post-fire	0.2640	1.4×10^{-5}	0.0138	-1.0×10^{-4}	0.0954	1.1×10^{-5}	0.4428	0.0010
12	Pre-fire	0.2357	1.4×10^{-5}	0.0361	-8.8×10^{-5}	0.2693	6.1×10^{-6}	0.3545	−0.0017
	Post-fire	0.1729	1.5×10^{-5}	0.0160	-1.3×10^{-4}	0.0500	1.4×10^{-5}	0.7890	−0.0004
13	Pre-fire	0.3266	-3.1×10^{-5}	0.6508	-2.3×10^{-5}	0.4972	-7.5×10^{-6}	0.8465	0.0003
	Post-fire	0.0418	7.3×10^{-5}	0.1425	-1.3×10^{-4}	0.0006	4.8×10^{-5}	1.0000	0.0000
14	Pre-fire	0.1347	2.9×10^{-5}	0.0053	-1.3×10^{-4}	0.1525	1.3×10^{-5}	0.1579	−0.0022
	Post-fire	0.1868	3.1×10^{-5}	0.0459	-1.5×10^{-4}	0.1911	1.7×10^{-5}	0.7450	−0.0005
15	Pre-fire	0.7949	4.3×10^{-6}	0.3155	-3.8×10^{-5}	0.8710	-1.7×10^{-6}	0.9611	−0.0002
	Post-fire	0.8203	7.1×10^{-6}	0.0001	-2.4×10^{-4}	0.2179	1.3×10^{-5}	0.1623	−0.0019
16	Pre-fire	0.0791	3.7×10^{-5}	0.3579	-5.6×10^{-5}	0.2125	1.0×10^{-5}	0.5720	−0.0008
	Post-fire	0.0501	5.2×10^{-5}	0.0000	-3.2×10^{-4}	0.0001	3.8×10^{-5}	0.6102	−0.0007
17	Pre-fire	0.8380	4.5×10^{-6}	0.5877	-3.8×10^{-5}	0.3507	1.7×10^{-5}	0.5877	−0.0010
	Post-fire	0.2235	1.7×10^{-5}	0.5907	-1.6×10^{-5}	0.6064	4.5×10^{-6}	0.0357	0.0023
18	Pre-fire	0.5522	-9.0×10^{-6}	0.0543	-7.4×10^{-5}	0.9145	-8.9×10^{-7}	0.0067	−0.0031
	Post-fire	0.6143	-5.5×10^{-6}	0.9601	-1.7×10^{-6}	0.5717	-3.8×10^{-6}	0.8807	0.0002
19	Pre-fire	0.0257	-3.6×10^{-5}	0.2877	3.1×10^{-5}	0.0288	-1.9×10^{-5}	0.3853	0.0010
	Post-fire	0.0000	4.4×10^{-5}	0.0002	-6.3×10^{-5}	0.0001	2.2×10^{-5}	0.8053	−0.0002
20	Pre-fire	0.6870	-8.3×10^{-6}	0.0391	-9.9×10^{-5}	0.4647	-7.7×10^{-6}	0.1007	−0.0030
	Post-fire	0.2263	1.4×10^{-5}	0.2450	4.0×10^{-5}	0.4989	5.2×10^{-6}	0.1016	0.0021
21	Pre-fire	0.7185	-9.0×10^{-6}	0.1056	-1.0×10^{-4}	0.8932	-2.4×10^{-6}	0.1435	−0.0027
	Post-fire	0.4281	-1.0×10^{-5}	0.3928	2.3×10^{-5}	0.5107	-4.3×10^{-6}	0.3175	0.0014

5.3. Effects of Burn Severity on Regrowth

5.3.1. Snowstorm

The LME analysis evaluating the impact of burn severity on post-fire LST revealed no significant effect of burn severity ($p > 0.05$). However, a significant temporal decrease in LST was detected (slope = −0.00056291, $p \leq 0.05$), highlighting a consistent decline over time. Similarly, when comparing LST trends inside and outside the fire perimeter, no significant spatial effect was found ($p > 0.05$). Despite this, a significant temporal decrease in LST was observed (slope = −0.00056198, $p \leq 0.05$), demonstrating a uniform reduction across both spatial locations. These findings emphasize that post-fire LST changes were predominantly driven by temporal dynamics rather than burn severity or spatial differences. The model had an AIC of 11,345 and a BIC of 11,384, whereas the LME model comparing points spatially had an AIC of 11,341 and a BIC of 11,369.

A comparable trend was observed in the analysis of the NDVI. The LME model assessing the effect of burn severity on the post-fire NDVI showed no significant overall

impact ($p > 0.05$), with none of the burn severity categories (moderate–high severity, moderate–low severity, or outside) exhibiting significant effects ($p > 0.05$). However, a significant temporal increase in the NDVI was detected (slope = 1.24×10^{-5}, $p \leq 0.05$), indicating consistent vegetation recovery over time. Similarly, NDVI trends inside and outside the fire perimeter showed no significant spatial effect ($p > 0.05$), but a significant temporal increase (slope = 1.23×10^{-5}, $p \leq 0.05$) confirmed that vegetation recovery occurred uniformly across both spatial locations. These results suggest that post-fire NDVI changes were primarily driven by temporal factors rather than burn severity or spatial differences. The model had an AIC of -7375.8 and a BIC of -7334.1, whereas the LME model comparing points spatially had an AIC of -7398.6 and a BIC of -7368.8.

The analysis of the MSI followed a similar pattern. The LME model assessing the effect of burn severity on the post-fire MSI found no significant overall impact ($p > 0.05$), with none of the burn severity categories exhibiting significant effects. However, a significant temporal decrease in the MSI was observed (slope = -3.96×10^{-5}, $p \leq 0.05$), suggesting that reductions in the MSI were primarily driven by temporal dynamics. Additionally, the comparison of MSI trends inside and outside the fire perimeter revealed no significant spatial effect ($p > 0.05$), yet a significant temporal decrease in the MSI (slope = -3.97×10^{-5}, $p \leq 0.05$) indicated a consistent decline across both spatial locations. These findings reinforce the conclusion that MSI changes post fire were predominantly influenced by time rather than spatial variation. The model had an AIC of 15.749 and a BIC of 57.472, whereas the LME model comparing points spatially had an AIC of -2.3245 and a BIC of 27.481.

A similar pattern was also observed for MCARI2. The LME analysis examining the effect of burn severity on post-fire MCARI2 showed no significant overall impact ($p > 0.05$), with none of the burn severity categories exhibiting significant effects ($p > 0.05$). However, a significant temporal increase in MCARI2 was detected (slope = 9.77×10^{-6}, $p \leq 0.05$), indicating consistent post-fire recovery of vegetation. Likewise, when comparing MCARI2 trends inside and outside the fire perimeter, no significant spatial effect was found ($p > 0.05$). Nevertheless, a significant temporal increase (slope = 9.77×10^{-6}, $p \leq 0.05$) suggested that vegetation recovery occurred uniformly across both spatial locations. These results further support the conclusion that post-fire MCARI2 changes were primarily driven by temporal dynamics rather than burn severity or spatial differences. The model had an AIC of -7277 and a BIC of -7238.6, whereas the LME model comparing points spatially had an AIC of -7302.1 and a BIC of -7274.7.

5.3.2. South Sugar Loaf

The LME analysis examining the effect of burn severity on post-fire LST showed no significant overall impact ($p > 0.05$). However, a significant reduction in LST was observed in areas of low severity (estimate = -1.203, $p \leq 0.05$), indicating effects of low burn severity on land surface. Despite this, no significant temporal trends in LST were identified (slope = -0.000194, $p > 0.05$), suggesting minimal influence from long-term changes. Similarly, when comparing LST trends inside and outside the fire perimeter, a significant effect of spatial location was detected ($p \leq 0.05$), but there were no significant temporal trends observed (slope = 0.000156, $p > 0.05$). These results indicate that post-fire LST changes were not predominantly driven by burn severity or temporal dynamics but instead reflected localized variations in specific burn severity categories. The model had an AIC of 9723.3 and a BIC of 9765.8, whereas the LME model comparing points spatially had an AIC of 11,524 and a BIC of 11,551.

A slightly different pattern emerged in the analysis of the NDVI. While the overall effect of burn severity on the post-fire NDVI was not significant ($p > 0.05$), significant increases were observed in areas of low severity (estimate = 0.0173, $p \leq 0.05$) and unburned

areas (estimate = 0.0201, $p \leq 0.05$). Additionally, a significant temporal increase in the NDVI (slope = 2.01×10^{-5}, $p \leq 0.05$) was detected, indicating a consistent trend of vegetation recovery over time. These findings suggest that while temporal dynamics played a dominant role in NDVI recovery, effects of low burn severity in regrowth were evident. However, when comparing NDVI trends inside and outside the fire perimeter, no significant effect of spatial location was found ($p > 0.05$), and no significant temporal trends were detected (slope = 5.58×10^{-7}, $p > 0.05$). This lack of spatial distinction suggests that vegetation recovery patterns were relatively uniform, with no clear differences between burned and unburned areas. The model had an AIC of −3206.4 and a BIC of −3163.9, whereas the LME model comparing points spatially had an AIC of −3870.5 and a BIC of −3843.

A similar pattern was observed in the analysis of the MSI. The effect of burn severity on the post-fire MSI was not significant overall ($p > 0.05$), yet a significant reduction in the MSI was noted in moderate–high-severity areas (estimate = −0.064, $p \leq 0.05$). This impact was accompanied by a strong temporal decrease in the MSI (slope = -1.61×10^{-4}, $p \leq 0.05$), suggesting that reductions in the MSI were mainly driven by time rather than burn severity. The LME analysis comparing MSI trends inside and outside the fire perimeter also found no significant effect of spatial location ($p > 0.05$). However, a significant temporal decrease in the MSI (slope = -1.18×10^{-4}, $p \leq 0.05$) indicated that reductions occurred consistently across both spatial locations. These results reinforce the idea that post-fire MSI changes were predominantly influenced by temporal dynamics, with some localized effects in more severely burned areas. The model had an AIC of 394.4 and a BIC of 429.08, whereas the LME model comparing points spatially had an AIC of 409.61 and a BIC of 436.17.

Unlike for the other indices, the LME analysis for MCARI2 revealed a significant overall impact of burn severity ($p \leq 0.05$). Significant increases in MCARI2 were observed in areas of low severity (estimate = 0.0091, $p \leq 0.05$), moderate–low severity (estimate = 0.0075, $p \leq 0.05$), and unburned areas (estimate = 0.0108, $p \leq 0.05$), indicating that burn severity influenced post-fire MCARI2 levels in specific categories. Additionally, a significant temporal increase in MCARI2 (slope = 1.33×10^{-5}, $p \leq 0.05$) suggested a steady recovery of vegetation over time. When comparing MCARI2 trends inside and outside the fire perimeter, no significant effect of spatial location was found ($p > 0.05$). However, a significant temporal increase (slope = 1.34×10^{-5}, $p \leq 0.05$) indicated consistent recovery across both spatial locations. These results suggest that post-fire MCARI2 changes were primarily driven by temporal dynamics, though localized burn severity effects were evident in certain categories. The model had an AIC of −5514.6 a and BIC of −5472.1, whereas the LME model comparing points spatially had an AIC of −5537.4 and a BIC of −5510.8.

6. Discussion

6.1. Burn Severity Analysis

The dNBR results for the Snowstorm and South Sugar Loaf fires reveal distinct patterns in burn severity distributions, reflecting variations in fire behavior and ecological responses. For the Snowstorm Fire, the majority of the affected area (74%) experienced low-severity burns, suggesting limited damage to vegetation and a higher likelihood of rapid recovery. In contrast, the South Sugar Loaf Fire exhibited a greater extent of high-severity burns (32%) and moderately high-severity burns (33%), indicating more significant vegetation loss and potentially slower recovery. These findings align with previous research emphasizing how fire intensity and severity shape post-fire vegetation dynamics [31]. The dominance of low-severity burns in the Snowstorm Fire is likely due to the presence of fire-adapted vegetation types, such as sagebrush steppe, which are resilient to lower-intensity fires [44].

These results have important implications for restoration planning. High-severity burn areas in the South Sugar Loaf Fire require targeted interventions, such as erosion

control measures or reseeding, to support recovery and prevent long-term degradation. On the other hand, areas affected by low-severity burns may recover naturally, highlighting the importance of mapping burn severity to guide restoration priorities effectively.

6.2. Spectral Indices Interpretation

The analysis of LST trends revealed notable differences between the two fire sites. In the Snowstorm Fire, a shift from upward trends pre fire to downward trends post fire was observed, suggesting cooling effects likely driven by vegetation regrowth and changes in surface albedo [45]. Conversely, the South Sugar Loaf Fire exhibited mixed post-fire LST trends, with localized reductions in low-severity areas pointing to the role of surviving vegetation in moderating surface temperatures.

The lack of significant spatial effects in both fires underscore the dominant influence of temporal recovery processes over spatial variability. These findings emphasize the need for ongoing monitoring to fully capture the thermal dynamics of post-fire landscapes and their implications for ecosystem resilience.

6.3. Normalized Difference Vegetation Index (NDVI)

NDVI trends following both fires indicated consistent increases over time, signaling vegetation recovery. For the Snowstorm Fire, recovery appeared uniform across all severity classes, while the South Sugar Loaf Fire showed more pronounced increases in low-severity and unburned areas. This observation aligns with studies demonstrating faster regrowth in areas affected by low-severity burns, where belowground root systems often survive and support recovery [46].

The significant temporal increase in the NDVI ($p < 0.001$) highlights the resilience of fire-adapted ecosystems in both regions. However, the absence of significant spatial variability in NDVI trends suggests that factors such as precipitation and temperature may play a more critical role than burn severity in influencing recovery trajectories. This is consistent with previous research emphasizing the importance of climatic conditions in shaping post-fire vegetation dynamics [47].

6.4. Moisture Stress Index (MSI)

MSI analysis revealed consistent downward trends both pre and post fire, reflecting reduced vegetation water stress over time. Significant temporal decreases in the MSI ($p < 0.001$) in both fires point to gradual improvements in plant moisture content, likely driven by vegetation regrowth and associated cooling effects. However, localized reductions in the MSI in moderate–high-severity areas of the South Sugar Loaf Fire ($p = 0.014$) indicate that these areas remain more vulnerable to prolonged moisture stress [48].

These results suggest that restoration efforts should prioritize areas with moderate–high- and high-severity burns to mitigate long-term stress and support ecosystem recovery. The use of water stress indicators, such as the MSI, in fire management strategies can enhance the effectiveness of restoration initiatives.

MCARI2 trends exhibited significant temporal increases in both fires, indicating consistent improvements in vegetation vigor and chlorophyll content during recovery. The unique sensitivity of MCARI2 to burn severity in the South Sugar Loaf Fire ($p = 0.014$) suggests that areas with low- and moderate–low-severity burns experienced faster recovery in comparison to high-severity burn areas, likely due to surviving vegetation and greater nutrient availability.

Unlike broader indices such as the NDVI, which reflect general vegetation properties (e.g., canopy cover and density), MCARI2 is specifically designed to capture variations in chlorophyll content and photosynthetic activity. This specificity enables MCARI2 to detect subtle differences in vegetation recovery that may not be apparent through other

indices [22]. For example, low-severity burns often preserve more photosynthetically active vegetation, resulting in higher MCARI2 values compared to areas with high-severity burns, where vegetation is more extensively consumed.

The dominance of shrubland and coniferous vegetation in the South Sugar Loaf Fire area likely contributed to MCARI2′s distinct response. These vegetation types exhibit varying recovery rates depending on burn severity, with low-severity burns facilitating faster regrowth and higher chlorophyll content. Additionally, environmental factors such as soil nutrient availability and post-fire precipitation patterns may have amplified chlorophyll-related variability detectable by MCARI2, further distinguishing it from indices like the NDVI or MSI. These findings underscore the value of MCARI2 in post-fire monitoring frameworks to capture nuanced recovery patterns and guide targeted restoration efforts.

Integrating the NDVI, MCARI2, MSI, and LST results provides a cohesive assessment of post-fire vegetation recovery across both the Snowstorm and South Sugar Loaf fires. Together, these indices offer complementary insights: increasing NDVI and MCARI2 values indicate rising canopy greenness and chlorophyll content, while declining MSI and LST values reflect reduced moisture stress and surface temperatures. The convergence of these trends suggests synchronous improvements in vegetation health, water availability, and surface energy balance, underscoring consistent recovery trajectories. In areas where indices diverge, such as high-severity patches in the South Sugar Loaf Fire, slower recovery in the NDVI and MCARI2 and elevated MSI values point to delayed physiological regrowth and sustained stress, further supported by limited LST reductions. In contrast, the Snowstorm Fire, dominated by low-severity burns, exhibited uniform improvements across all indices. This integrated interpretation enhances understanding of both spatial variability and overall ecosystem resilience, offering a more comprehensive view of post-fire recovery than any individual index alone.

6.5. Generalizability and Monitoring Implications

The findings of this study highlight the versatility of remote sensing indices in monitoring post-fire vegetation recovery across diverse ecosystems. While this research focused on two specific wildfire events, the methodologies and indices applied, such as the dNBR, NDVI, MSI, and MCARI2, are broadly applicable to other fire-affected landscapes. These indices offer scalable and cost-effective tools for assessing vegetation dynamics across regions with varying climatic, ecological, and fire regime characteristics. However, it is important to acknowledge that spectral indices alone provide generalized information and may not capture critical structural attributes of vegetation. For instance, the NDVI is prone to saturation in areas with dense canopy cover, limiting its sensitivity in high biomass conditions [49], while the MSI can be influenced by soil background reflectance, particularly in arid or sparsely vegetated environments [50]. Therefore, for more detailed characterization of vegetation structure, particularly in forested ecosystems, the integration of multispectral imagery with LiDAR is recommended, as LiDAR provides essential three-dimensional structural data [51,52]. Such fusion allows for deeper insights into vegetation recovery processes, including the distinction between native regrowth and invasive species colonization. By demonstrating the effectiveness of integrating multiple spectral indices, this study provides a foundation for standardized post-fire monitoring practices while recognizing the value of complementary data sources in advancing global vegetation recovery assessments.

The results of this study provide valuable insights into the recovery dynamics of fire-affected ecosystems. The consistent influence of temporal trends across all indices highlights the importance of long-term monitoring for understanding recovery trajectories.

The observed variations in recovery rates between low- and high-severity areas emphasize the need for targeted restoration strategies that address localized vulnerabilities.

From a land management perspective, these findings demonstrate the utility of remote sensing metrics in guiding post-fire interventions. Burn severity maps can help prioritize areas requiring immediate restoration, while indices such as the NDVI and MSI can track recovery progress. Incorporating tools like MCARI2, which can detect fine-scale variations in vegetation health, can further enhance the effectiveness of fire management strategies and support sustainable ecosystem recovery.

6.6. Future Directions

Future research should focus on understanding the interaction of burn severity with topography, precipitation, and vegetation type to comprehensively explore the effects of burn severity. The study should be expanded to multiple wildfires across the same ecosystem and varied ecosystems to enhance the effects of burn severity on different vegetation types and ecosystems.

7. Conclusions

This study demonstrates that changes over time are the primary drivers of post-wildfire vegetation recovery, as evidenced by significant increases in the NDVI and MCARI2 and corresponding decreases in the MSI. These trends indicate consistent vegetation re-growth across both wildfire events. Specifically, significant year-to-year increases in the NDVI and MCARI2, alongside declines in the MSI, indicate a progressive improvement in vegetation health and structure during the study period. These trends reflect systematic ecological responses to wildfire disturbances, such as regrowth and increased vegetation density and chlorophyll content, as time progresses due to precipitation and other climatic factors. While temporal dynamics were more influential than spatial location or categorical burn severity in explaining post-fire vegetation changes, burn severity still exerted a localized influence. Areas affected by moderate- and low-severity burns recovered more rapidly, likely due to the survival of root systems and improved nutrient cycling. The influence of the vegetation type and fire regime was also notable, as ecosystems with fire-adapted species showed greater resilience.

The remote sensing indices employed in this study, namely the NDVI, MSI, MCARI2, and LST, proved effective in capturing different aspects of vegetation health following fires. These results highlight the importance of prioritizing restoration efforts in high-severity burn areas to prevent soil degradation and promote ecological recovery. Furthermore, the methodology demonstrated in this study is scalable and applicable to other fire-prone regions. Overall, the findings underscore the value of integrating multiple spectral indices for global post-fire vegetation monitoring and emphasize the importance of long-term observations in supporting effective ecosystem management and resilience-building in fire-affected landscapes.

Author Contributions: Conceptualization, I.A. and H.S.; methodology, I.A.; software, I.A.; formal analysis, I.A.; investigation, I.A.; writing—original draft preparation, I.A.; writing—review and editing, I.A. and H.S.; visualization, I.A.; supervision, H.S.; project administration, H.S.; funding acquisition, H.S. All authors have read and agreed to the published version of the manuscript.

Funding: This research was funded by National Science Foundation under grant number OIA-2148788 and the APC was funded by the same grant.

Data Availability Statement: The datasets generated and/or analyzed during the current study are fully presented in the published article. No additional datasets were generated or used.

Conflicts of Interest: The authors declare no conflict of interest.

References

1. Bowd, E.J.; Banks, S.C.; Strong, C.L.; Lindenmayer, D.B. Long-Term Impacts of Wildfire and Logging on Forest Soils. *Nat. Geosci.* **2019**, *12*, 113–118. [CrossRef]
2. Ebel, B.A. Temporal Evolution of Measured and Simulated Infiltration Following Wildfire in the Colorado Front Range, USA: Shifting Thresholds of Runoff Generation and Hydrologic Hazards. *J. Hydrol.* **2020**, *585*, 124765. [CrossRef]
3. Francos, M.; Úbeda, X.; Pereira, P.; Alcañiz, M. Long-Term Impact of Wildfire on Soils Exposed to Different Fire Severities. A Case Study in Cadiretes Massif (NE Iberian Peninsula). *Sci. Total Environ.* **2018**, *615*, 664–671. [CrossRef]
4. Johnstone, J.F.; Allen, C.D.; Franklin, J.F.; Frelich, L.E.; Harvey, B.J.; Higuera, P.E.; Mack, M.C.; Meentemeyer, R.K.; Metz, M.R.; Perry, G.L.; et al. Changing Disturbance Regimes, Ecological Memory, and Forest Resilience. *Front. Ecol. Environ.* **2016**, *14*, 369–378. [CrossRef]
5. Lee, J.H. Prediction of Large-Scale Wildfires With the Canopy Stress Index Derived from Soil Moisture Active Passive. *IEEE J. Sel. Top. Appl. Earth Obs. Remote Sens.* **2021**, *14*, 2096–2102. [CrossRef]
6. van Leeuwen, W.J.D.; Casady, G.M.; Neary, D.G.; Bautista, S.; Alloza, J.A.; Carmel, Y.; Wittenberg, L.; Malkinson, D.; Orr, B.J. Monitoring Post-Wildfire Vegetation Response with Remotely Sensed Time-Series Data in Spain, USA and Israel. *Int. J. Wildland Fire* **2010**, *19*, 75–93. [CrossRef]
7. Tian, Y.; Wu, Z.; Li, M.; Wang, B.; Zhang, X. Forest Fire Spread Monitoring and Vegetation Dynamics Detection Based on Multi-Source Remote Sensing Images. *Remote Sens.* **2022**, *14*, 4431. [CrossRef]
8. Ahmad, I.; Stephen, H.; Ahmad, S. Machine Learning-Based Land Cover Classification and Impact Assessment in Pre-Wildfire and Post-Wildfire Areas. In Proceedings of the World Environmental and Water Resources Congress 2024, Milwaukee, WI, USA, 19–22 May 2024; pp. 1572–1582. [CrossRef]
9. Avetisyan, D.; Velizarova, E.; Filchev, L. Post-Fire Forest Vegetation State Monitoring through Satellite Remote Sensing and In Situ Data. *Remote Sens.* **2022**, *14*, 6266. [CrossRef]
10. Shvetsov, E.G.; Kukavskaya, E.A.; Buryak, L.V.; Barrett, K. Assessment of Post-Fire Vegetation Recovery in Southern Siberia Using Remote Sensing Observations. *Environ. Res. Lett.* **2019**, *14*, 055001. [CrossRef]
11. Ahmad, I.; Aslam, S.; Hussain, U. Assessment of Plastic Pollution in Coastal Areas of Karachi: Case Study of West Warf, Kemari Jetty, and Manora. *Mar. Pollut. Bull.* **2023**, *195*, 115501. [CrossRef]
12. Yi, K.; Tani, H.; Zhang, J.; Guo, M.; Wang, X.; Zhong, G. Long-Term Satellite Detection of Post-Fire Vegetation Trends in Boreal Forests of China. *Remote Sens.* **2013**, *5*, 6938–6957. [CrossRef]
13. Miller, J.D.; Thode, A.E. Quantifying Burn Severity in a Heterogeneous Landscape with a Relative Version of the Delta Normalized Burn Ratio (dNBR). *Remote Sens. Environ.* **2007**, *109*, 66–80. [CrossRef]
14. Velizarova, E.; Nedkov, R.; Avetisyan, D.; Radeva, K.; Stoyanov, A.; Georgiev, N.; Gigova, I. Application of Remote Sensing Techniques for Monitoring of the Climatic Parameters in Forest Fire Vulnerable Regions in Bulgaria. In Proceedings of the Seventh International Conference on Remote Sensing and Geoinformation of the Environment (RSCy2019), Paphos, Cyprus, 18–21 March 2019; SPIE: Bellingham, WA, USA, 2019; Volume 11174, pp. 451–462.
15. Xofis, P.; Buckley, P.G.; Takos, I.; Mitchley, J. Long Term Post-Fire Vegetation Dynamics in North-East Mediterranean Ecosystems. The Case of Mount Athos Greece. *Fire* **2021**, *4*, 92. [CrossRef]
16. Verbesselt, J.; Hyndman, R.; Zeileis, A.; Culvenor, D. Phenological Change Detection While Accounting for Abrupt and Gradual Trends in Satellite Image Time Series. *Remote Sens. Environ.* **2010**, *114*, 2970–2980. [CrossRef]
17. Wang, Q.; Adiku, S.; Tenhunen, J.; Granier, A. On the Relationship of NDVI with Leaf Area Index in a Deciduous Forest Site. *Remote Sens. Environ.* **2005**, *94*, 244–255. [CrossRef]
18. Coops, N.C.; Waring, R.H.; Landsberg, J.J. Assessing Forest Productivity in Australia and New Zealand Using a Physiologically-Based Model Driven with Averaged Monthly Weather Data and Satellite-Derived Estimates of Canopy Photosynthetic Capacity. *For. Ecol. Manag.* **1998**, *104*, 113–127. [CrossRef]
19. Myneni, R.B.; Hoffman, S.; Knyazikhin, Y.; Privette, J.L.; Glassy, J.; Tian, Y.; Wang, Y.; Song, X.; Zhang, Y.; Smith, G.R.; et al. Global Products of Vegetation Leaf Area and Fraction Absorbed PAR from Year One of MODIS Data. *Remote Sens. Environ.* **2002**, *83*, 214–231. [CrossRef]
20. Richard, Y.; Poccard, I. A Statistical Study of NDVI Sensitivity to Seasonal and Interannual Rainfall Variations in Southern Africa. *Int. J. Remote Sens.* **1998**, *19*, 2907–2920. [CrossRef]
21. Schloss, A.L.; Kicklighter, D.W.; Kaduk, J.; Wittenberg, U.; The Participants of the Potsdam NpP Model Intercomparison. Comparing Global Models of Terrestrial Net Primary Productivity (NPP): Comparison of NPP to Climate and the Normalized Difference Vegetation Index (NDVI). *Glob. Change Biol.* **1999**, *5*, 25–34. [CrossRef]
22. Haboudane, D.; Miller, J.R.; Pattey, E.; Zarco-Tejada, P.J.; Strachan, I.B. Hyperspectral Vegetation Indices and Novel Algorithms for Predicting Green LAI of Crop Canopies: Modeling and Validation in the Context of Precision Agriculture. *Remote Sens. Environ.* **2004**, *90*, 337–352. [CrossRef]

23. Stankova, N.; Nedkov, R.; Ivanova, I.; Avetisyan, D. Modeling of Forest Ecosystems Recovery after Fire Based on Orthogonalization of Multispectral Satellite Data. In Proceedings of the Earth Resources and Environmental Remote Sensing/GIS Applications IX, Berlin, Germany, 11–13 September 2018; SPIE: Bellingham, WA, USA, 2018; Volume 10790, pp. 426–432.
24. Daughtry, C.S.T.; Walthall, C.L.; Kim, M.S.; de Colstoun, E.B.; McMurtrey, J.E. Estimating Corn Leaf Chlorophyll Concentration from Leaf and Canopy Reflectance. *Remote Sens. Environ.* **2000**, *74*, 229–239. [CrossRef]
25. Zhao, X.; Cao, C.; Ni, X.; Chen, W. Retrieval and Application of Leaf Area Index over China Using HJ-1 Data. *Geomat. Nat. Hazards Risk* **2017**, *8*, 478–495. [CrossRef]
26. Cao, X.; Cui, X.; Yue, M.; Chen, J.; Tanikawa, H.; Ye, Y. Evaluation of Wildfire Propagation Susceptibility in Grasslands Using Burned Areas and Multivariate Logistic Regression. *Int. J. Remote Sens.* **2013**, *34*, 6679–6700. [CrossRef]
27. Schut, A.G.T.; Stephens, D.J.; Stovold, R.G.H.; Adams, M.; Craig, R.L.; Schut, A.G.T.; Stephens, D.J.; Stovold, R.G.H.; Adams, M.; Craig, R.L. Improved Wheat Yield and Production Forecasting with a Moisture Stress Index, AVHRR and MODIS Data. *Crop Pasture Sci.* **2009**, *60*, 60–70. [CrossRef]
28. Avdan, U.; Jovanovska, G. Algorithm for Automated Mapping of Land Surface Temperature Using LANDSAT 8 Satellite Data. *J. Sens.* **2016**, *2016*, 1480307. [CrossRef]
29. Kuenzer, C.; Dech, S. *Thermal Infrared Remote Sensing: Sensors, Methods, Applications*; Springer Science & Business Media: Berlin/Heidelberg, Germany, 2013; ISBN 978-94-007-6639-6.
30. Vlassova, L.; Pérez-Cabello, F.; Mimbrero, M.R.; Llovería, R.M.; García-Martín, A. Analysis of the Relationship between Land Surface Temperature and Wildfire Severity in a Series of Landsat Images. *Remote Sens.* **2014**, *6*, 6136–6162. [CrossRef]
31. Key, C.H.; Benson, N.C. *Landscape Assessment (LA)*; U.S. Department of Agriculture, Forest Service, Rocky Mountain Research Station: Fort Collins, CO, USA, 2006.
32. United States Geological Survey. *US Forest Service; Kurtis Nelson Burn Severity Portal, a Clearing House of Fire Severity and Extent Information (Ver. 9.0, October 2024)*; United States Geological Survey: Reston, VA, USA, 2024.
33. Freden, S.C.; Mercanti, E.P.; Becker, M.A. *Third Earth Resources Technology Satellite-1 Symposium: Section A-B. Technical Presentations*; Scientific and Technical Information Office, National Aeronautics and Space Administration: Hampton, VA, USA, 1974.
34. Rock, B.N.; Vogelmann, J.E.; Williams, D.L.; Vogelmann, A.F.; Hoshizaki, T. Remote Detection of Forest Damage: Plant Responses to Stress May Have Spectral "Signatures" That Could Be Used to Map, Monitor, and Measure Forest Damage. *BioScience* **1986**, *36*, 439–445. [CrossRef]
35. Dudek, G. STD: A Seasonal-Trend-Dispersion Decomposition of Time Series. *IEEE Trans. Knowl. Data Eng.* **2023**, *35*, 10339–10350. [CrossRef]
36. Li, C.; Jia, X.; Zhu, R.; Mei, X.; Wang, D.; Zhang, X. Seasonal Spatiotemporal Changes in the NDVI and Its Driving Forces in Wuliangsu Lake Basin, Northern China from 1990 to 2020. *Remote Sens.* **2023**, *15*, 2965. [CrossRef]
37. Leys, C.; Ley, C.; Klein, O.; Bernard, P.; Licata, L. Detecting Outliers: Do Not Use Standard Deviation around the Mean, Use Absolute Deviation around the Median. *J. Exp. Soc. Psychol.* **2013**, *49*, 764–766. [CrossRef]
38. Kendall, M.G. *Rank Correlation Methods*; Rank correlation methods; Griffin: Oxford, UK, 1948.
39. Mann, H.B. Nonparametric Tests Against Trend. *Econometrica* **1945**, *13*, 245–259. [CrossRef]
40. Sen, P.K. Estimates of the Regression Coefficient Based on Kendall's Tau. *J. Am. Stat. Assoc.* **1968**, *63*, 1379–1389. [CrossRef]
41. Wainwright, P.E.; Leatherdale, S.T.; Dubin, J.A. Advantages of Mixed Effects Models over Traditional ANOVA Models in Developmental Studies: A Worked Example in a Mouse Model of Fetal Alcohol Syndrome. *Dev. Psychobiol.* **2007**, *49*, 664–674. [CrossRef] [PubMed]
42. Yu, Z.; Guindani, M.; Grieco, S.F.; Chen, L.; Holmes, T.C.; Xu, X. Beyond t Test and ANOVA: Applications of Mixed-Effects Models for More Rigorous Statistical Analysis in Neuroscience Research. *Neuron* **2022**, *110*, 21–35. [CrossRef]
43. Luke, S.G. Evaluating Significance in Linear Mixed-Effects Models in R. *Behav. Res.* **2017**, *49*, 1494–1502. [CrossRef]
44. Balch, J.K.; Bradley, B.A.; D'Antonio, C.M.; Gómez-Dans, J. Introduced Annual Grass Increases Regional Fire Activity across the Arid Western USA (1980–2009). *Glob. Change Biol.* **2013**, *19*, 173–183. [CrossRef]
45. Chudnovsky, A.; Ben-Dor, E.; Saaroni, H. Diurnal Thermal Behavior of Selected Urban Objects Using Remote Sensing Measurements. *Energy Build.* **2004**, *36*, 1063–1074. [CrossRef]
46. Johnstone, J.F.; Chapin, F.S.; Hollingsworth, T.N.; Mack, M.C.; Romanovsky, V.; Turetsky, M. Fire, Climate Change, and Forest Resilience in Interior Alaska. *Can. J. For. Res.* **2010**, *40*, 1302–1312. [CrossRef]
47. Abatzoglou, J.T.; Kolden, C.A. Relationships between Climate and Macroscale Area Burned in the Western United States. *Int. J. Wildland Fire* **2013**, *22*, 1003–1020. [CrossRef]
48. Klein, J.A.; Harte, J.; Zhao, X.-Q. Dynamic and Complex Microclimate Responses to Warming and Grazing Manipulations. *Glob. Change Biol.* **2005**, *11*, 1440–1451. [CrossRef]
49. Asrar, G.; Fuchs, M.; Kanemasu, E.T.; Hatfield, J.L. Estimating Absorbed Photosynthetic Radiation and Leaf Area Index from Spectral Reflectance in Wheat. *Agron. J.* **1984**, *76*, 300–306. [CrossRef]

50. Hunt, E.R.; Rock, B.N. Detection of Changes in Leaf Water Content Using Near- and Middle-Infrared Reflectances. *Remote Sens. Environ.* **1989**, *30*, 43–54. [CrossRef]
51. Asner, G.P.; Knapp, D.E.; Kennedy-Bowdoin, T.; Jones, M.O.; Martin, R.E.; Boardman, J.; Hughes, R.F. Invasive Species Detection in Hawaiian Rainforests Using Airborne Imaging Spectroscopy and LiDAR. *Remote Sens. Environ.* **2008**, *112*, 1942–1955. [CrossRef]
52. Dubayah, R.O.; Drake, J.B. Lidar Remote Sensing for Forestry. *J. For.* **2000**, *98*, 44–46. [CrossRef]

Disclaimer/Publisher's Note: The statements, opinions and data contained in all publications are solely those of the individual author(s) and contributor(s) and not of MDPI and/or the editor(s). MDPI and/or the editor(s) disclaim responsibility for any injury to people or property resulting from any ideas, methods, instructions or products referred to in the content.